INVESTIGATING THE ATOMIC INTERACTIONS OF FLEXIBLE ORGANIC SOLAR CELLS

Author: Jennifer Mejia Old Dominion University- Department of Chemistry

Abstract

Solar technology is an integral component of the electrical power systems of most spacecraft produced by NASA. Top-performing solar panels have reached record-high efficiencies but require intricate and expensive manufacturing. The technology used to advance these systems also adds undesirable weight and restricts the diversity of their applications because of their rigidity. These limitations make promising alternatives, like organic solar cells (OSCs), viable options to investigate. While OSCs have excellent tunability, are lightweight, and have improved power conversions, efficiencies are not yet competitive against other solar cell types. Many performance pitfalls result from poor carrier mobility across networks within the device's active layers. Improved characterization methodologies are critical to understanding the barriers to improved performance. We use solid-state nuclear magnetic resonance (ssNMR) and x-ray diffraction (XRD) to investigate critical structural features that govern intermolecular interactions within OSC materials. The data obtained here provide valuable insight into the competitive role that intermolecular interactions play in the packing patterns, a powerful performance indicator observed in these systems.

1. Introduction

Solar panels are a vital power source for NASA spacecraft.[1] Current photovoltaic devices have heavier weights that limit the amount of productive cargo these spacecraft can house, like fuel and instrumentation. Organic-type solar cell (OSC) materials are merging to the forefront of viable alternatives because of their lighter weights and high specific power ratings.[2] Even with lower power conversion efficiencies compared to current systems, interest in this growing field has expanded in the last 20 years, for these devices are lightweight and highly tunable.[3]

Although variables like assembly technique and heat contribute to OSC performance, the "active layer" is arguably the largest area of opportunity for improvement.[4]

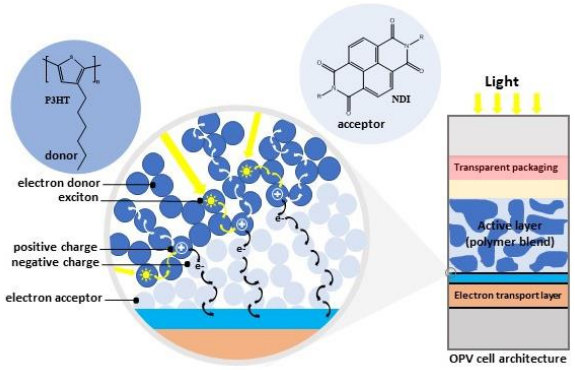

Figure 1. OSC device architecture and active layer

This region in the solar cell, where light absorption and electron transport occur, typically comprises mixtures of small organic molecules and conductive polymers.[5] Successful light absorption and charge transport are a product of the various atomic interactions between these mixtures.[6] As a result, molecules used in these cells are chosen because of their structural features, like π-π stacking, and potential charge carrying capacity.[7,8]

π-stacking interactions play a crucial role in the morphology of OSCs and contribute to charge mobility. Unfortunately, the most common analytical methods for characterizing amorphous systems lack the spatial resolution to investigate the relationship between structure and these interactions' role on device performance.[9] The complexity of these samples makes using more powerful techniques like x-ray diffraction (XRD) or solution nuclear magnetic resonance (NMR) extremely difficult.[10] Specifically, OSC blends do not have the required long-range order for XRD,

and dissolving samples for solution NMR causes a total loss of structural features in cast cells. Consequently, developing a new methodology to explore and improve our understanding of the relationship between unique structural features is an essential step towards controlling the nanostructural morphology of the active layer and eventually improving their efficiencies.[11,12]

High-resolution solid-state NMR (ssNMR) is well suited for characterizing complex materials like OSC systems.[13–15] Unlike solution NMR where molecular tumbling of dissolved samples results in a single isotropic chemical shift, ssNMR samples are packed as-is for observation and allow for examining a wide variety of samples. As a result, spectral signals reflect the local environment of the sample, which helps examine the local structure of materials like amorphous blends in OSC systems.[16–17] Combined with other characterization methods, routine ssNMR has the potential to identify morphology and local packing within OSC blends.

Here, we use a multi-technique approach to demonstrate the π-stacking of OSC acceptor materials. The first series, dialkyl N, N'-naphthalene diimide (NDI) molecules, the simplest π-stacking prototype, were synthesized and characterized via solution and solid-state NMR. Following the NDI analysis, a second set of molecules, dialkyl N, N' -perylene diimide (PDI) molecules, were synthesized.

In the first series, the NDIs were synthesized using modified literature procedures[19–21].

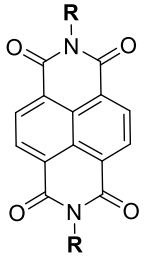

H for NDI-amide **(H)**
CH_4 for NDI-methyl **(Me)**
C_2H_6 for NDI-ethyl **(Et)**
C_3H_8 for NDI-propyl **(Pr)**
C_4H_{10} for NDI-butyl **(Bu)**
C_5H_{12} for NDI-pentyl **(Pe)**
C_6H_{14} for NDI-hexyl **(Hex)**
C_7H_{16} for NDI-heptyl **(Hep)**
C_8H_{18} for NDI-octyl **(Oct)**
$C_{10}H_{22}$ for NDI-decyl **(Dec)**
$C_{12}H_{26}$ for NDI-dodecyl **(Dodec)**
$C_{14}H_{30}$ for NDI-tetradecyl **(Tet)**

Scheme 1. Chemical structure of NDIx molecules.

The second series, the PDIs, were synthesized using similar procedures to the NDIs.

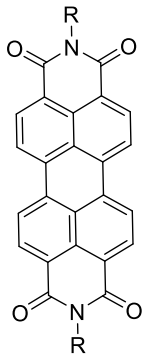

H for NDI-amide **(H)**
CH_4 for NDI-methyl **(Me)**
C_2H_6 for NDI-ethyl **(Et)**
C_3H_8 for NDI-propyl **(Pr)**
C_4H_{10} for NDI-butyl **(Bu)**
C_5H_{12} for NDI-pentyl **(Pe)**
C_6H_{14} for NDI-hexyl **(Hex)**
C_7H_{16} for NDI-heptyl **(Hep)**
C_8H_{18} for NDI-octyl **(Oct)**
$C_{10}H_{22}$ for NDI-decyl **(Dec)**
$C_{12}H_{26}$ for NDI-dodecyl **(Dodec)**
$C_{14}H_{30}$ for NDI-tetradecyl **(Tet)**

Scheme 2. Chemical structure of PDIx molecules

2. Experimental

Solid-state NMR spectroscopy

All ^{13}C NMR analyses were performed on a Bruker Avance II 400 spectrometer at 100 MHz for ^{13}C. Samples were packed in 4-mm-diameter zirconia rotors with Kel-F caps, and experiments were run in a double-resonance probe head, and the rotor was spun at the magic angle of 54.7° to the direction of the magnetic field. The ^{13}C chemical shifts were referenced to tetramethylsilane (TMS), with ^{13}COO-labeled glycine at 176.49 ppm as a secondary reference.

2.2.2 X-ray Crystallography

Crystals suitable for X-ray analyses were grown by solvent diffusion from chloroform solution. All measurements were made by

Robert D. Pike of William and Mary University in Williamsburg, VA using microfocus Cu Kα radiation on a Bruker-AXS three-circle Apex DUO diffractometer equipped with a SMART Apex II CCD detector. The full dataset was collected at 100 K or 296 K.

Crystal structures available for analysis were found in the CSD database[22–30]

3. Results and Discussion

Systematic determination of π-stacking modes using ssNMR began with synthesizing and purifying the above NDIs. Peak splitting and integration values confirmed symmetric imidization of both anhydrides of the starting dianhydride. Additionally, singlet peaks representing the four aromatic protons of all NDIs are evidence of no substitutions on the naphthalene core.

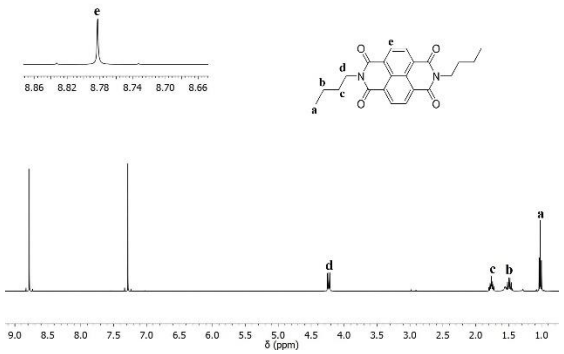

Figure. 2 ^{1}H spectrum of NDI-butyl from solution NMR. The zoomed-in region between 8.60-9.00 ppm showed the aromatic singlet peak, e, representing the NDI's four core protons and was observed in all synthesized NDIs.

Subsequently, NDIs were prepared for ssNMR, and resultant spectra were separated into three regions for analysis: (1) aliphatic, (2) aromatic, and (3) carbonyl (Figure).

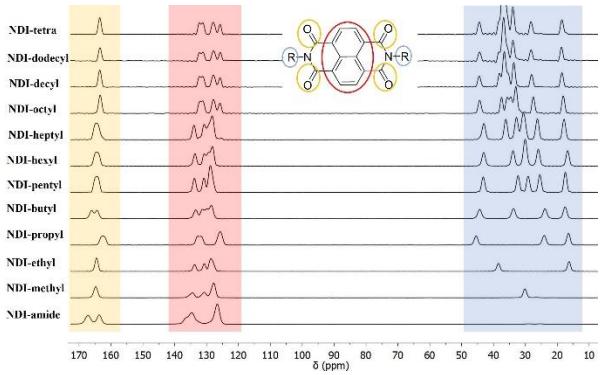

Figure 3. ^{13}C multiCP/MAS ssNMR spectra of NDIs. Three spectral regions: aliphatic (blue), aromatic (red), and carbonyl (orange).

The aliphatic resonances in ^{13}C multiCP/MAS spectra (0-50 ppm) are comparable to the corresponding solution NMR spectra. However, the NDI aromatic regions (125-138 ppm) had unusual peak patterns and chemical shift differences.

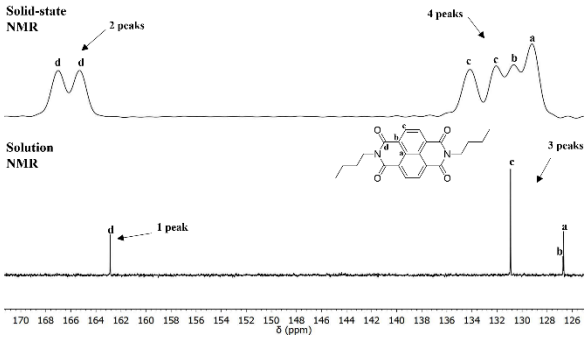

Figure 4. ^{13}C multiCP/MAS spectrum of NDI-butyl (top) and ^{13}C solution NMR spectrum of NDI-butyl (bottom).

Interestingly, distinct patterns could be identified in the aromatic ^{13}C multiCP/MAS region (Figure). This suggests that the similar spectra for groups of NDIs could be attributed to a similar packing environment giving rise to a similar chemical environment.

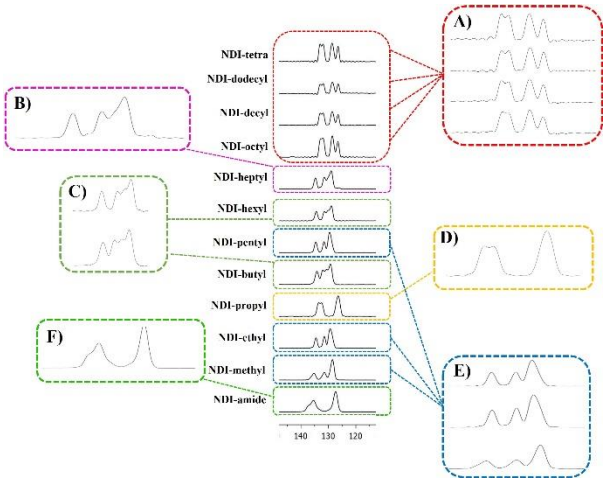

Figure 5. ^{13}C multiCP/MAS of NDIs from 120-140 ppm. NDIs were categorized based on spectral appearance due to the commonalities between their chemical shift differences.

NDIs could be separated into two groups based on the chemical shifts of their carbonyl signals. Short-chain NDIs-methyl-heptyl had downfield peaks around ~165 ppm, and long-chain NDIs octyl-tetradecyl were more upfield by 1-2 ppm. NDI-propyl had the most upfield carbonyl peak at 163.53 ppm. Additionally, NDIs-amide and butyl had two carbonyl signals, suggesting that the effect of crystal packing for these two is not limited to the aromatic regions but extends to the carbonyl chemical environments.

Further characterization of the NDI aromatic environments was probed using ^{1}H-^{13}C 2D HETCOR ssNMR. Signals in ^{1}H-^{13}C HetCor spectra reveal carbons correlated to protons via dipolar or through space coupling.

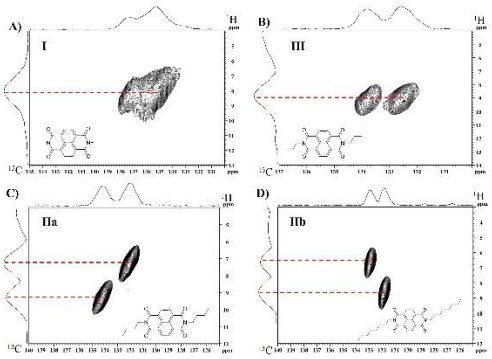

Figure 6. ^{1}H-^{13}C Hetcor spectra of the aromatic region of selected NDIs (CP = 75 µs).

X-ray structures were obtained either from crystals grown from synthesized NDIs or the CCDC database. Due to strong π-π interactions, all NDI crystal structures pack in columns with the molecules parallel dis-placed (PD) and twisted (TW) along the column axis. Four packing orientations were identified in the NDIs. (Figure).

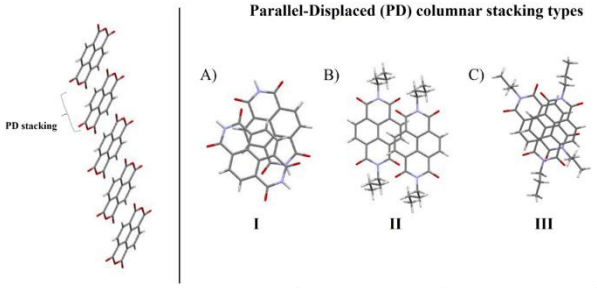

Figure 7. XRD crystal structures of NDIs. On the left is an example of a single column where stacking refers to the way two adjacent molecules come together. There were three PD types: A) PD and twisted (I), B) PD (II), and C) twisted (III).

3.3 ssNMR Prediction

To demonstrate the predictive potential of ssNMR, 1D and 2D spectra were collected for isoamyl-NDI, for which the X-ray structure was unknown.

^{13}C multiCP/MAS spectra of NDI-isoamyl had the same aromatic spectral appearance as Type E. HetCor patterns were similar to PD IIa 2D NMRs.

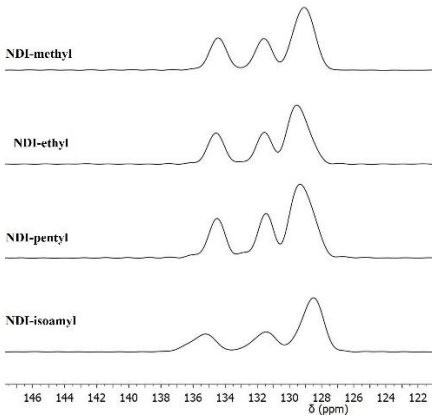

Figure 8. Comparison of 1D 13C multiCP/MAS of NDIs methyl, ethyl, pentyl, and isoamyl.

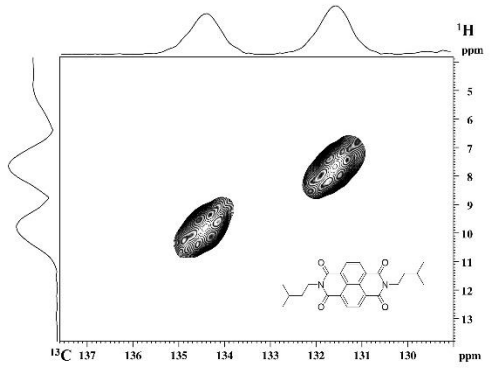

Figure 9. 1H-13C 2D HetCor spectrum of NDI-isoamyl with CP of 75 µs.

Following ssNMR, XRD results confirmed the proposed similarities, demonstrating our ability to use ssNMR to predict packing patterns, a practical application when examining the potential performance of amorphous films where XRD is inappropriate.

Various structural features of molecules, such as electronegativity or hydrogen bonding, influence the magnitude of the magnetic field experienced by a particular nucleus. The nature of these features causes atoms to appear at different chemical shifts on a spectrum. In ssNMR, samples are prepared directly into rotors without solvents, so molecules do not randomly tumble in a liquid like in solution NMR, influencing nuclear NMR interactions and their corresponding spectra. Specifically, in solids, the magnetic moments of nuclear spins are so close that they can interact with each other through space, and molecules are in all molecular orientations. Therefore, in ssNMR, chemical shifts are anisotropic and orientation dependent.

When placed in the magnet, the π electrons of the NDI aromatic systems influenced the chemical shifts of aromatic carbons differently in ssNMR compared to solution NMR. These chemical shift differences resulted from the inherent anisotropy and depended on where the carbon atom stacked within a neighboring molecule's ring current. If, in the solid state, a carbon packed within the ring current and another outside, then the molecule's symmetry was broken and caused different peaks to appear for atoms no longer considered equivalent.

In the case of the NDIs with lower chemical shifts in both aromatic and carbonyl regions, the upfield signals of both carbon and carbonyl peaks show that the atoms of these regions experience the strength of the magnetic field less intensely than those with downfield signals. Since the aliphatic regions of these atoms are not similarly influenced, and only regions close to the π system are impacted, it can be deduced that in the upfield NDIs, the arrangement of molecules results in increased shielding and π interactions.

Since π-stacking plays a significant role in the properties of materials, it is an important consideration when examining the OSC active layer. Since OSCs now utilize complex molecular systems with increasingly complex networks and film morphologies, examining these π-systems was expanded to include a series of PDI molecules. This portion of the project is still ongoing, as the imidization of the anhydride produced precipitates with blends of the starting material and reagents. Extending the π-system in the PDIs reduced solubility and made for complex purification. Following many attempts, we found that running reactions for longer reaction times provided pure PDIs. The overall physical appearance and texture of the PDIs make them challenging to run in ssNMR.

Despite the complexity of the PDIs π-system, preliminary results show similar packing predictions as with NDIs.

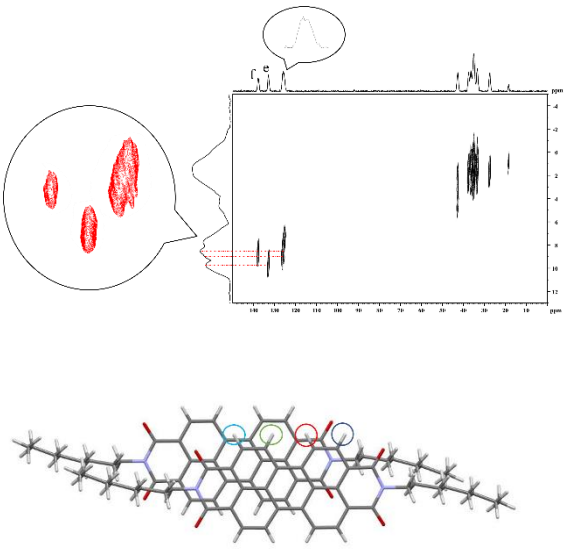

Figure 10. ^{1}H-^{13}C HetCor spectrum of PDI-octyl and corresponding crystal structure.

From the HetCor, we see four unique chemical environments for the aromatic protons of the PDI. Two carbons are near the ring current, and two are further downfield outside the ring current. Even with the molecule's symmetry, we see four unique environments. The impact of packing on the system's chemical environment is similar to the NDI systems.

Future work will include the completion of PDI ssNMR and XRD analysis. Following this, we will proceed to examine blended systems of both NDI and PDIs with the regioregular polymer poly(3-hexylthiophene-2,5-diyl), P3HT.

References:

(1) Green, C. M.; Lomask, M. *Project Vanguard: The NASA History*, Dover ed.; Dover Publications: Mineola, N.Y, 2009.

(2) Reb, L. K.; Böhmer, M.; Predeschly, B.; Grott, S.; Dreißigacker, C.; Drescher, J.; Meyer, A.; Müller-Buschbaum, P. An Experiment for Novel Material Thin-Film Solar Cell Characterization on Sounding Rocket Flights. *Review of Scientific Instruments* **2021**, *92* (7), 074501. https://doi.org/10.1063/5.0047346.

(3) Chen, L. X. Organic Solar Cells: Recent Progress and Challenges. *ACS Energy Lett.* **2019**, *4* (10), 2537–2539. https://doi.org/10.1021/acsenergylett.9b02071.

(4) 25th Anniversary Article: Bulk Heterojunction Solar Cells: Understanding the Mechanism of Operation - Heeger - 2014 - Advanced Materials - Wiley Online Library https://onlinelibrary.wiley.com/doi/abs/10.1002/adma.201304373 (accessed 2022 -04 -09).

(5) Nowak-Król, A.; Shoyama, K.; Stolte, M.; Würthner, F. Naphthalene and Perylene Diimides – Better Alternatives to Fullerenes for Organic Electronics? *Chem. Commun.* **2018**, *54* (98), 13763–13772. https://doi.org/10.1039/C8CC07640E.

(6) Benanti, T. L.; Venkataraman, D. Organic Solar Cells: An Overview Focusing on Active Layer Morphology. *Photosynth Res* **2006**, *87* (1), 73–81. https://doi.org/10.1007/s11120-005-6397-9.

(7) Li, H.; Sini, G.; Sit, J.; Moulé, A. J.; Bredas, J.-L. Understanding Charge Transport in Donor/Acceptor Blends from Large-Scale Device Simulations Based on Experimental Film Morphologies. *Energy Environ. Sci.* **2020**, *13* (2), 601–615. https://doi.org/10.1039/C9EE03791H.

(8) Menke, S. M.; Ran, N. A.; Bazan, G. C.; Friend, R. H. Understanding Energy Loss in Organic Solar Cells: Toward a New Efficiency Regime. *Joule* **2018**, *2* (1), 25–35. https://doi.org/10.1016/j.joule.2017.09.020.

(9) Bryce, D. L. NMR Crystallography: Structure and Properties of Materials

from Solid-State Nuclear Magnetic Resonance Observables. *IUCrJ* **2017**, *4* (4), 350–359. https://doi.org/10.1107/S2052252517006042.

(10) Vanlaeke, P.; Swinnen, A.; Haeldermans, I.; Vanhoyland, G.; Aernouts, T.; Cheyns, D.; Deibel, C.; D'Haen, J.; Heremans, P.; Poortmans, J.; Manca, J. V. P3HT/PCBM Bulk Heterojunction Solar Cells: Relation between Morphology and Electro-Optical Characteristics. *Solar Energy Materials and Solar Cells* **2006**, *90* (14), 2150–2158. https://doi.org/10.1016/j.solmat.2006.02.010.

(11) Nieuwendaal, R. C.; Snyder, C. R.; DeLongchamp, D. M. Measuring Order in Regioregular Poly(3-Hexylthiophene) with Solid-State 13C CPMAS NMR. *ACS Macro Lett.* **2014**, *3* (2), 130–135. https://doi.org/10.1021/mz4005343.

(12) Measuring the Degree of Crystallinity in Semicrystalline Regioregular Poly(3-hexylthiophene) | Macromolecules https://pubs.acs.org/doi/10.1021/acs.macromol.6b00799 (accessed 2022 -04 -09).

(13) Mao, J.; Cao, X.; Olk, D. C.; Chu, W.; Schmidt-Rohr, K. Advanced Solid-State NMR Spectroscopy of Natural Organic Matter. *Progress in Nuclear Magnetic Resonance Spectroscopy* **2017**, *100*, 17–51. https://doi.org/10.1016/j.pnmrs.2016.11.003.

(14) Mao, J.; Kong, X.; Schmidt-Rohr, K.; Pignatello, J. J.; Perdue, E. M. Advanced Solid-State NMR Characterization of Marine Dissolved Organic Matter Isolated Using the Coupled Reverse Osmosis/Electrodialysis Method. *Environ. Sci. Technol.* **2012**, *46* (11), 5806–5814. https://doi.org/10.1021/es300521e.

(15) R. Luginbuhl, B.; Raval, P.; Pawlak, T.; Du, Z.; Wang, T.; Kupgan, G.; Schopp, N.; Chae, S.; Yoon, S.; Yi, A.; Jung Kim, H.; Coropceanu, V.; Brédas, J.; Nguyen, T.; Reddy, G. N. M. Resolving Atomic-Scale Interactions in Nonfullerene Acceptor Organic Solar Cells with Solid-State NMR Spectroscopy, Crystallographic Modelling, and Molecular Dynamics Simulations. *Advanced Materials* **2022**, *34* (6), 2105943. https://doi.org/10.1002/adma.202105943.

(16) Duer, M. J. *Introduction to Solid-State NMR Spectroscopy*; Blackwell: Oxford, UK ; Malden, MA, 2004.

(17) Levitt, M. H. *Spin Dynamics: Basics of Nuclear Magnetic Resonance*, 2nd ed.; John Wiley & Sons: Chichester, England ; Hoboken, NJ, 2008.

(18) Ye, L.; Zhao, W.; Li, S.; Mukherjee, S.; Carpenter, J. H.; Awartani, O.; Jiao, X.; Hou, J.; Ade, H. High-Efficiency Nonfullerene Organic Solar Cells: Critical Factors That Affect Complex Multi-Length Scale Morphology and Device Performance. *Adv. Energy Mater.* **2017**, *7* (7), 1602000. https://doi.org/10.1002/aenm.201602000.

(19) Ofir, Y.; Zelichenok, A.; Yitzchaik, S. 1,4;5,8-Naphthalene-Tetracarboxylic Diimide Derivatives as Model Compounds for Molecular Layer Epitaxy. *J. Mater. Chem.* **2006**, *16* (22), 2142–2149. https://doi.org/10.1039/B601258B.

(20) Shukla, D.; Welter, T. R. N-Type Semiconductor Materials in Thin Film Transistors. WO2009126203A1, October 15, 2009.

(21) Iscrulescu, L.; Sebe, I.; Atanasoaie, D.; Tantaveanu, E.; Mîndruta, C. New Xanthene Structures. *Revista de Chimie* **2008**, *59* (5), 578–0.

(22) Meillaud, F.; Shah, A.; Droz, C.; Vallat-Sauvain, E.; Miazza, C. Efficiency Limits for Single-Junction and Tandem Solar Cells. *Solar Energy Materials and Solar Cells* **2006**, *90* (18), 2952–2959. https://doi.org/10.1016/j.solmat.2006.06.002.

(23) Pandeeswar, M.; Khare, H.; Ramakumar, S.; Govindaraju, T. Biomimetic Molecular Organization of Naphthalene Diimide in the Solid State: Tunable (Chiro-) Optical, Viscoelastic and Nanoscale Properties. *RSC Adv.* **2014**, *4* (39), 20154–20163. https://doi.org/10.1039/C3RA47257D.

(24) Krishna, G. R.; Devarapalli, R.; Lal, G.; Reddy, C. M. CCDC 1029340: Experimental Crystal Structure Determination, 2016. https://doi.org/10.5517/CCDC.CSD.CC13K3J9.

(25) Alvey, P. M.; Reczek, J. J.; Lynch, V.; Iverson, B. L. A Systematic Study of Thermochromic Aromatic Donor−Acceptor Materials. *J. Org. Chem.* **2010**, *75* (22), 7682–7690. https://doi.org/10.1021/jo101498b.

(26) Andric, G.; Boas, J. F.; Bond, A. M.; Fallon, G. D.; Ghiggino, K. P.; Hogan, C. F.; Hutchison, J. A.; Lee, M. A.-P.; Langford, S. J.; Pilbrow, J. R.; Troup, G. J.; Woodward, C. P. CCDC 238148: Experimental Crystal Structure Determination, 2005. https://doi.org/10.5517/CC7ZT66.

(27) Shukla, D.; Nelson, S. F.; Freeman, D. C.; Rajeswaran, M.; Ahearn, W. G.; Meyer, D. M.; Carey, J. T. Thin-Film Morphology Control in Naphthalene-Diimide-Based Semiconductors: High mobility n-Type Semiconductor for Organic Thin-Film Transistors. *Chem. Mater.* **2008**, *20* (24), 7486–7491. https://doi.org/10.1021/cm802071w.

(28) Milita, S.; Liscio, F.; Cowen, L.; Cavallini, M.; Drain, B. A.; Degousée, T.; Luong, S.; Fenwick, O.; Guagliardi, A.; Schroeder, B. C.; Masciocchi, N. Polymorphism in *N* , *N* ′-Dialkyl-Naphthalene Diimides. *J. Mater. Chem. C* **2020**, *8* (9), 3097–3112. https://doi.org/10.1039/C9TC06967D.

(29) Alvey, P. M.; Reczek, J. J.; Lynch, V.; Iverson, B. L. CCDC 819750: Experimental Crystal Structure Determination, 2011. https://doi.org/10.5517/CCWJ0KY.

(30) Lynch, D. E.; Hamilton, D. G. CCDC 230429: Experimental Crystal Structure Determination, 2004. https://doi.org/10.5517/CC7QS6X.